PROOF

Available online at www.sciencedirect.com

SCIENCE DIRECT®

Remote Sensing of Environment 96 (2005) 37–48

Remote Sensing of Environment

www.elsevier.com/locate/rse

Remote sensing of sunlight-induced chlorophyll fluorescence and reflectance of Scots pine in the boreal forest during spring recovery

Juliette Louis[a,*], Abderrahmane Ounis[a], Jean-Marc Ducruet[a], Sébastien Evain[a], Tuomas Laurila[b], Tea Thum[b], Mika Aurela[b], Gunnar Wingsle[c], Luis Alonso[d], Roberto Pedros[d], Ismaël Moya[a]

[a]*Laboratoire pour l'Utilisation du Rayonnement Electromagnétique (LURE) - CNRS, Univ. Paris-Sud, Bât. 203-BP34, 91898 Orsay, France*
[b]*Finnish Meteorological Institute (FMI), Climate and Global Change Research, Sahaajankatu 20E, FIN-00880, Helsinki, Finland*
[c]*Agricultural University, Department of Forest Genetics and Plant Physiology, SLU, SE-901 83 Umeå, Finland*
[d]*Universitat de València- Avda. Blasco Ibáñez, 13. 46010 València, Spain*

Received 17 September 2004; received in revised form 26 January 2005; accepted 29 January 2005

Abstract

A measurement campaign to assess the feasibility of remote sensing of sunlight-induced chlorophyll fluorescence (ChlF) from a coniferous canopy was conducted in a boreal forest study site (Finland). A Passive Multi-wavelength Fluorescence Detector (PMFD) sensor, developed in the LURE laboratory, was used to obtain simultaneous measurements of ChlF in the oxygen absorption bands, at 687 and 760 nm, and a reflectance index, the PRI (Physiological Reflectance Index), for a month during spring recovery. When these data were compared with active fluorescence measurements performed on needles they revealed the same trend. During sunny days fluorescence and reflectance signals were found to be strongly influenced by shadows associated with the canopy structure. Moreover, chlorophyll fluorescence variations induced by rapid light changes (due to transient cloud shadows) were found to respond more quickly and with larger amplitude under summer conditions compared to those obtained under cold acclimation conditions. In addition, ChlF at 760 nm was observed to increase with the chlorophyll content. During this campaign, the CO_2 assimilation was measured at the forest canopy level and was found remarkably well correlated with the PRI index.
© 2005 Elsevier Inc. All rights reserved.

Keywords: Boreal forest; Sunlight-induced chlorophyll fluorescence; CO_2 flux; Diurnal cycle; Oxygen absorption band; Passive remote sensing; FLD principle; PRI; Scots pine

1. Introduction

The boreal forest, composed of evergreen (pine and fir) and deciduous (birch and aspen) trees, contributes significantly to carbon fluxes since it is the largest forest of the northern hemisphere. Most conifers retain their needles for several years. Thus cold acclimation processes have been developed, that facilitate survival in severe freezing periods, sometimes combined with high light levels. Earlier studies performed at the needle level have shown that conifers in cold climates experience large seasonal changes in photosynthetic activity. They exhibit a gradual decline during late summer and autumn, a strong inhibition during winter, and a complete recovery during spring. A study of the carotenoid composition of the

Abbreviations: APAR; Absorbed photosynthetically active radiation; Chl; Chlorophyll; FIPAM; Frenquency induced pulse amplitude modulation; FLD; Fraunhofer line discriminator; Fo; minimum yield of Chl a fluorescence in dark-adapted needles; Fm; maximum yield of Chl a fluorescence in dark adapted needles; Fm'; maximum yield of Chl a fluorescence in the presence of PAR; Fs; stationary Chl fluorescence flux; Fv/Fm; maximum photochemical yield of PSII; ΔF/Fm'; effective photochemical yield; LHCII; Light harvesting antenna of photosystem II; Lidar; Light detection and ranging; NDVI; Normalized difference vegetation index; NPQ; Non-photochemical quenching; PAR; Photosynthetically active radiation; PMFD; Passive multi-wavelength fluorescence detector; PRI; Physiological reflectance index (also called Photochemical Reflectance Index); PSI; Photosystem I; PSII; Photosystem II; Q_A; primary quinone acceptor.

* Corresponding author. Tel.: +33 1 64 46 82 72; fax: +33 1 64 46 80 06.
E-mail address: Juliette_louis@uqtr.ca (J. Louis).

0034-4257/$ - see front matter © 2005 Elsevier Inc. All rights reserved.
doi:10.1016/j.rse.2005.01.013

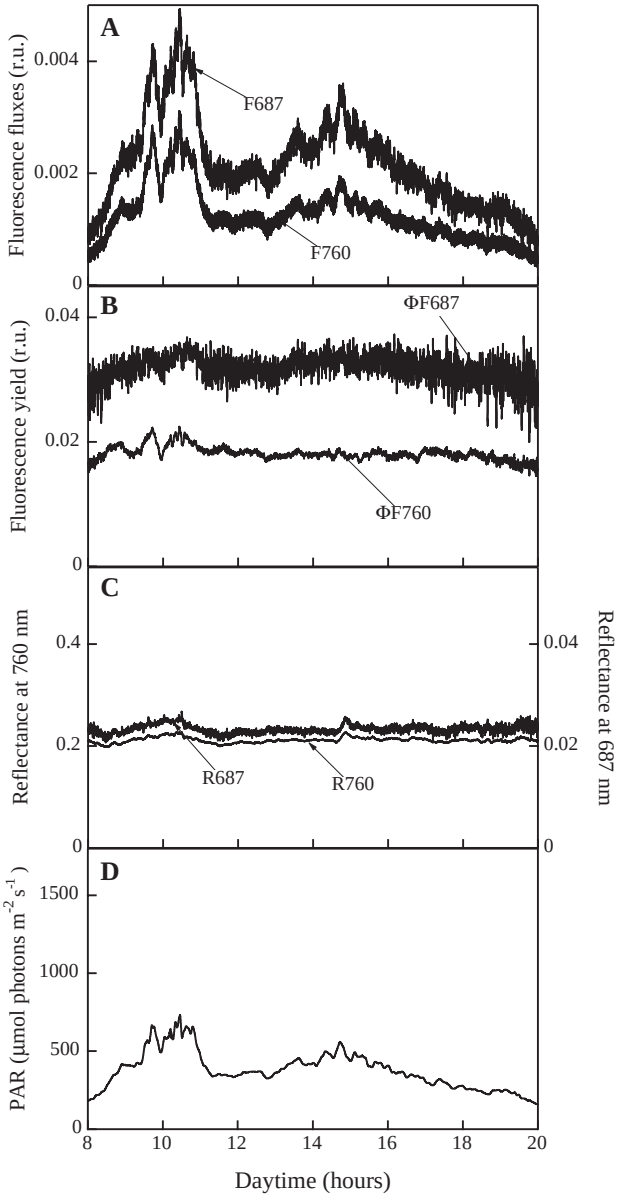

Fig. 6. Diurnal cycle variations of the PAR and of the fluorescence and reflectance measured by the PMFD for low light conditions (22 May 2002). (A) Fluorescence fluxes at 687 and 760 nm. (B) Fluorescence yields at 687 and 760 nm, obtained by dividing the fluorescence fluxes by the flux reflected by the target at 570 nm. (C) Reflectance at 687 and 760 nm. (D) PAR.

cence yield for each wavelength by dividing the fluorescence fluxes by the radiance reflected by the target at 570 nm, denoted by ΦF687 and ΦF760.

Fig. 5B shows that ΦF687 increased roughly from 8:00 to 20:00 local time, with a step transition after 14:00. In the same conditions, ΦF760 stayed fairly constant. For the same day, the reflectance at 687 nm was close to 4% and the reflectance at 760 nm was close to 30% (Fig. 5C). One can observe that these bi-directional reflectances increased at midday in a more pronounced way at 687 nm than at 760nm.

When diffuse light dominated, all signals, including PAR and radiances, had a similar shape (data not shown). The fluorescence fluxes closely followed PAR variations (compare Fig. 6A and D). The fluorescence yields, ΦF687 and ΦF760, were parallel and almost constant (Fig. 6B). When the PAR increased above 400 μmol m^{-2} s^{-1}, a slight increase of both yields was observed. The reflectance signals stayed constant over the day (Fig. 6C).

Fig. 7A shows a typical diurnal cycle of the PRI index together with the PAR. The variation was almost symmetric from morning to evening with a minimum around solar noon. Due to rapid succession of sun and shade periods, PRI variations were not clearly resolved except around 18:00 that day, when the transition is longer. Fig. 7B illustrates the response of PRI to PAR variations lasting several minutes. The PRI index is inversely correlated with PAR. A sudden transition lasting several minutes from full sunlight to overcast conditions induces an increase of PRI.

3.3. Evolution of the signals during the campaign

In order to follow the evolution of the signals during the campaign, time series have been generated by integrating the data between 11:00 and 15:00 local time for the fluorescence yields (Fig. 8A). Very cloudy days (PAR < 500 μmol photons m^{-2} s^{-1}) have been discarded.

One can observe that the daily integrated values of both ΦF687 and ΦF760 were positively correlated with the integrated PAR. ΦF760 showed a greater dynamic range,

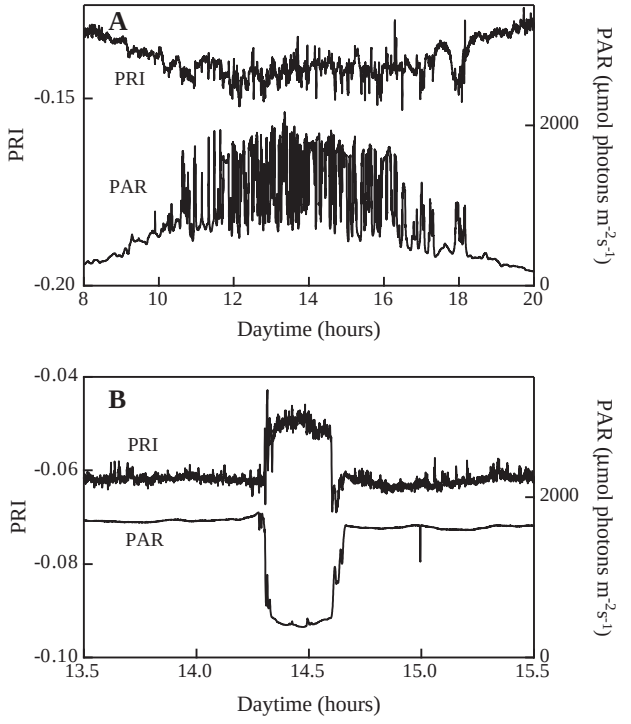

Fig. 7. (A) Typical diurnal cycle of the PRI index, measured by the PMFD, together with PAR (24 May 2002). (B) Decrease of the PRI index occurring after rapid transitions lasting several minutes from overcast to full sunlight (9 June 2002).

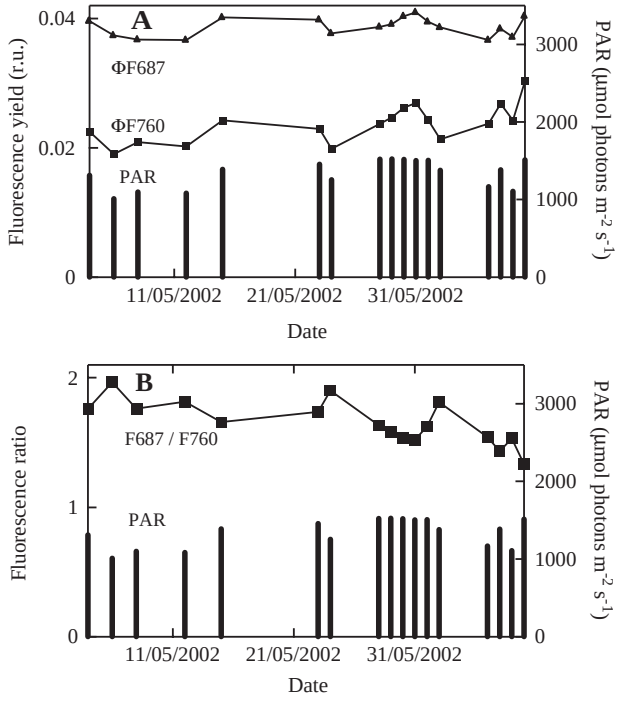

Fig. 8. (A) Time series of fluorescence yields and PAR integrated over 4 h around solar noon (14:00). Both yields were correlated with PAR (except for the sunny days at the end of May). Φ760 increased at the end of the campaign whereas Φ687 stayed fairly constant. (B) Time series of the fluorescence ratio (F687 / F760).

with an increase at the end of the campaign, whereas ΦF687 stayed almost constant. As a result, the ratio of the integrated yields, ΦF687/ΦF760 (=F687/F760), exhibited a continuous decrease more marked at the end of the campaign (Fig. 8B).

At the beginning of the campaign, on April 23–24, when there was still a continuous snow cover, negative net CO_2 fluxes of about -0.05 mg m^{-2} s^{-1} at noon were observed (Fig. 9A, B). The CO_2 uptake by the canopy was already exceeding the total respiration. After June 2, the net CO_2 fluxes at noon increased to -0.4 mg m^{-2} s^{-1}, which is a typical value in summer. A time series of net CO_2 assimilation was generated and plotted with the time series obtained for the PRI (Fig. 10). The sign of net CO_2 assimilation was changed so that the two signals could be compared. One can observe a good correlation between these signals as both remained almost constant until the end of May and then rose continuously up to the end of the campaign. The rise took place one day later for the net CO_2 assimilation. The PRI calculated from the data obtained with the ASD radiometer gave the same steep increase at the end of the campaign (data not shown).

Time series were also generated using active fluorescence measurements averaged between 11:00 and 15:00. Fv/Fm and ΔF/Fm' were plotted for each day (Fig. 11). Fv/Fm increased regularly during the whole period from 0.60 (6 May) to 0.80 (June). Independent measurements were made with the PEA instrument, starting from the beginning of April. At this date, Fv/Fm was below 0.2 and began to increase steeply at the end of April to reach 0.6 on the first week of May, which was in good agreement with the results obtained with the FIPAM (data not shown). ΔF/Fm' was continuously measured with the FIPAM during May and June. Fig. 11 shows a negative correlation between ΔF/Fm' and the averaged PAR. However, by selecting days having approximately the same low illumination (squares), one can observe a monotonic increase of the corresponding ΔF/Fm' values. The same observation can be made when selecting high light days (circles).

Due to the high temporal resolution of the PMFD (2 s), it was possible to compare fluorescence transients from full sunlight to cloudy conditions at the beginning and at the end of the campaign. Fluorescence yields were plotted versus PAR during short transition periods (<1 h) (Fig. 12A) during which the position of the sun could be considered almost constant. For clarity, a fit of the points is represented (Fig. 12B). In all cases fluorescence yield responded positively to PAR variations. The initial slope of these curves was calculated. Fig. 12C compares these fits for days at the beginning and at the end of the campaign. At 687 nm, we observed a 27% increase of the initial slope, whereas the fluorescence yield level under full sunlight was unchanged, as already stated (Fig. 8). At 760 nm, we observed a 42% increase of the initial slope. It is concluded that at both wavelengths the responsiveness of fluorescence yield to PAR variations is increased at the end of the campaign.

3.4. Pigment content

The total chlorophyll content remained almost constant except for a slight increase at the end of the period, whereas the Chlorophyll a/b ratio remained stable throughout the period (Table 1). A decrease of the carotenoid pool, more

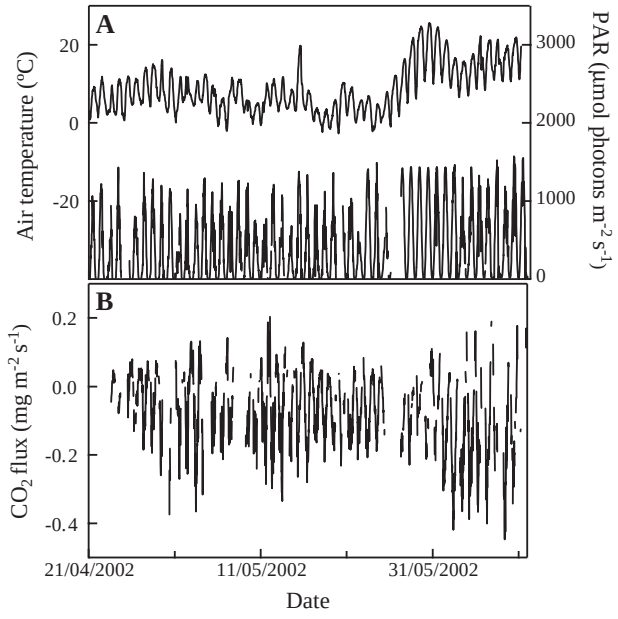

Fig. 9. (A) Air temperature (upper line) and PAR (lower line) on April 21–June 11. (B) Half hourly net CO_2 flux on April 21–June 11. A negative net CO_2 flux indicates net uptake (flux downward) by the forest.

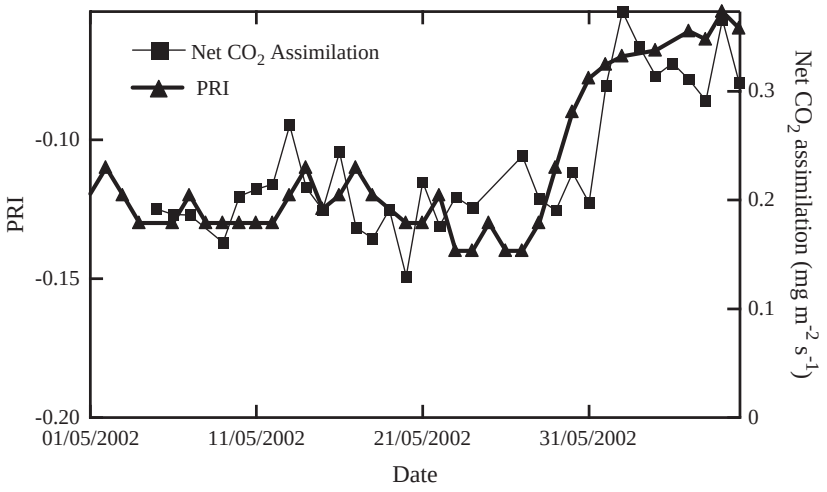

Fig. 10. Parallel plots of the PRI index and CO_2 uptake time series during the campaign. Observe the parallel increase at the end of May.

pronounced for the lutein pigment, could be observed. These findings are in good agreement with data reported in the literature for the boreal forest (Ottander et al., 1995).

4. Discussion

A prominent feature is obvious in the radiance data (Fig. 4). The shape of the radiance signals measured with the PMFD on sunny days is very different according to whether they originate from the reference or from the target. This difference is attributed to a different light interception between the 3D canopy and the 2D reference panel. The peak around 14:00, observed for all of the sunny days, is probably ascribable to a Hot Spot effect (Hapke et al., 1996; Kuusk, 1985) as the inclination angles of the instrument and the sun were respectively 30° and 42°, and the azimuthal angles were very close. The other irregularities could be due to a changing pattern of lighted and shadowed area of the tree canopy, when the direction of incident light changes. The sensitivity to the Hot Spot effect depends on the canopy reflection and transmission properties. At 687 nm, the signal is strongly absorbed and will arise mostly from the top of the target, and so will be more sensitive to Hot Spot effect than the signal at 760 nm, which is weakly absorbed and arises from scattering within the whole canopy. This may explain the more pronounced peak at 687 nm compared to 760 nm. The structural origin of these effects is confirmed by the data obtained under diffuse illumination conditions. In this case, all the radiance signals, from the target and from the reference, can almost be superimposed, and depend only on PAR variations.

The fluorescence fluxes follow the same propagation laws and so have the same shape as the corresponding radiant fluxes (Fig. 5A). The calculation of fluorescence yields was expected to minimize canopy structure effects and to simplify the interpretation of canopy fluorescence emission. However, the diurnal cycles acquired on sunny days with active and passive techniques are quite different (Figs. 3A and 5B).

4.1. Comparison of active and passive fluorescence measurements

The diurnal cycles measured on sunny days by the FIPAM are characterized by a pronounced decrease of Fs, under high light conditions, to a level lower than Fo (Fig. 3A). This decrease is attributed to the increase of the non-photochemical quenching (NPQ), calculated as stated above, which reached 2.5 at midday (not shown). This behaviour indicates that the plant was undergoing a strong constraint. As the campaign took place just after the snow melting period, a water deficit seems unlikely, so the reversible NPQ during the daily cycle is attributed to excess light.

At variance with Fs measured with the FIPAM, the diurnal cycles of both ΦF687 and ΦF760 recorded by the

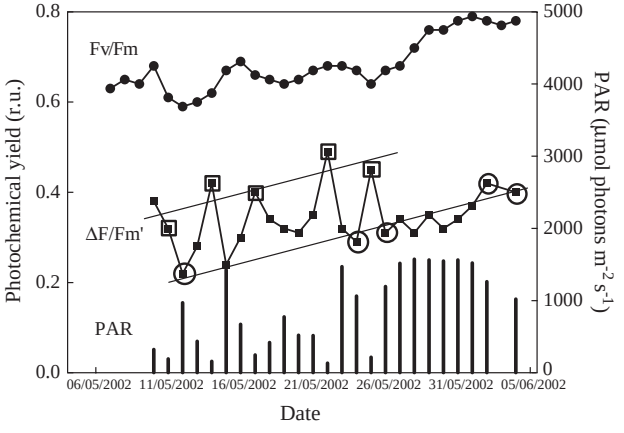

Fig. 11. Evolution of the PAR and of the maximal and effective photochemical yields during the campaign, measured by the FIPAM. The circles and the squares highlight the increase of ΔF/Fm' for the same PAR. Squares correspond to a PAR of about 200 µmol photons m^{-2} s^{-1}, circles to a PAR of about 1000 µmol photons m^{-2} s^{-1}.

PMFD for the same days do not show any decrease of ΦF at midday. This is interpreted as a very moderated contribution of NPQ. These discrepancies may arise from differences in the target structure. In the case of the active measurements, the needles are fixed, oriented towards the south, homogeneously and continuously illuminated, especially around solar noon. These unusual conditions probably generate the observed strong NPQ. In the case of passive measurements, the target is composed of several trees. Needles inside the canopy are shadowed by other needles or stems, either permanently or flickeringly. As a result, the average intensity they receive is lower and probably not sufficient to induce a detectable non-photochemical quenching effect. Only the permanently sun-exposed needles undergo a strong non-photochemical quenching and this contribution is diluted in the overall fluorescence emission of the canopy.

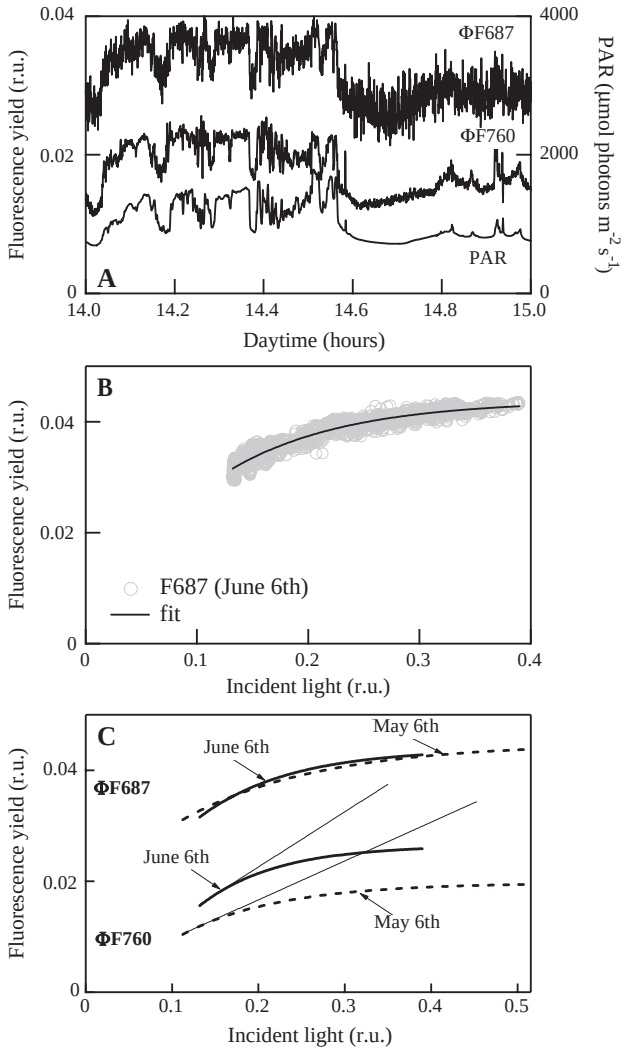

Fig. 12. Dynamical study of fluorescence. (A) Fluorescence yields at 687 and 760 nm and PAR plotted versus time (June 6th). (B) Fluorescence yield at 687 nm (June 6th) plotted versus incident light and the curve obtained by an exponential fit. (C) Comparison of the fitted curves at 687 and 760 nm for a day at the beginning of the campaign, May 6th, and a day at the end of the campaign, June 6th. The initial tangents are represented for the curves at 760 nm.

Table 1
Chlorophyll, xanthophyll cycle carotenoids and lutein content, at the beginning (May 8th) and at the end (June 12th) of the campaign

	Chl a+Chl b (μg/g DW)	Chl a / Chl b	Xanthophyll pool (μg/g DW)	Lutein (μg/g DW)
May 8th	2500	3.1	86.7	141
June 12th	2900	3.4	60.6	92.5

4.2. Evolution of the signals during spring recovery

The structural effects make the interpretation of the diurnal cycles of the passive measurements more difficult. However the calculation of time series alleviates this problem and reveals the evolution of the fluorescence signals during spring recovery. The time series obtained with the PMFD (Fig. 8) show that the fluorescence yields variations were parallel to the PAR variations: this is a typical characteristic of plants under weak constraints. On the other hand, the negative correlation of ΔF/Fm' with the PAR, observed for active measurements (Fig. 11) is rather indicative of a light constraint. Again this may be explained by the structural effects and the difference in the illumination of the target, as already discussed.

Considering the temporal evolution of fluorescence yields, we observed that ΦF687 stayed almost constant during the campaign, while ΦF760 increased, particularly at the end of the campaign. The increase of ΦF760 could be related to the increase of the Chl content during the campaign (see Table 1). One can hypothesize that the fluorescence flux is proportional to the absorbed PAR, which depends on the total Chl amount. As the fluorescence at 760 nm is not re-absorbed by the Chl, we expected an increase when the Chl amount increases (Gitelson et al., 1999). The situation is different at 687 nm, which is a wavelength strongly absorbed. In that case, F687 is saturated even for low Chl concentrations. As a result we do not expect any increase of ΦF687, in agreement with the observation. The effect of the Chl concentration increase is better evidenced on the F687/F760 ratio which exhibited a continuous decrease, more marked at the end of the campaign (Fig. 8B). No significant change was observed on the temporal evolution of the NDVI index (not shown), indicating a lower sensitivity of this index compared to fluorescence.

Fig. 12C shows the dynamical response of Chl fluorescence to the variations of incident light. This response contains the variations of the Chl fluorescence yields in response to the change of ambient light and also fluorescence induction transitions occurring after very rapid light changes. The increase of the initial slope (ΔF/ΔPAR) between the beginning and the end of the campaign is interpreted as a reduction of the mechanisms of non radiative energy dissipation, which maintain a low Chl

fluorescence yield under cold acclimated conditions. In addition to ΔpH associated NPQ, these mechanisms include long-term sustained quenching for the whole winter period (Öquist & Huner, 2003). This last quenching mechanism affects both radiative and photochemical energy dissipation pathways. It is well documented that a plant under constraint is often characterized by a lower light threshold for the apparition of the NPQ. As a result, a lower Fs is observed for a given light level (Cerovic et al., 1996; Flexas et al., 2000; Günther et al., 1994). However in the present case, the change observed during the campaign concerns mainly the long-term quenching associated with cold acclimation.

Although active and passive measurements were performed with different targets and illumination conditions, the fluorescence parameters measured with these two techniques reveal the same evolution during the campaign. Indeed, the time series obtained with the FIPAM confirmed the previous conclusion. Fig. 11 shows an increasing level of the maximal photochemical yield (Fv/Fm) and hence an increase of the photosynthetic activity. These findings were corroborated by the time series of the net CO_2 assimilation (Fig. 10). The effective electron transfer rate (ΔF/Fm), that was measured continuously during the campaign, also shows the same trend. It is necessary for this to consider separately low light and high light conditions as shown in Fig. 11.

One can conclude that interesting information on the photosynthetic capacity of the vegetation is contained in naturally-induced fluorescence variations, which can be accessed by passive fluorescence remote sensing.

Another interesting result is the good correlation between the PRI index and the net CO_2 assimilation (Fig. 10). The PRI index is associated with two identified mechanisms, involved in excess light dissipation as heat. The first one corresponds to rapid changes in the aggregation state of antenna chlorophyll–protein complexes induced by the energisation of the thylakoid membrane. It is accompanied by absorbance changes centered near 531–535 nm (Bilger et al., 1989; Ruban et al., 1993). The second one corresponds to the dynamic changes in the de-epoxidation state of the xanthophyll cycle, which are accompanied by absorbance changes at 505–515 nm (Bilger et al., 1989; Heber, 1969; Heber et al., 1986; Krause, 1973; Li et al., 2000). The absorption changes generate a broad reflectance change around 531 nm, including both mechanisms (Gamon et al., 1990). The robustness of this correlation was strengthened in a recent work on grape vines (Evain et al., 2004), which demonstrated the existence of two phases. A rapid phase lasting less than 2 s consists in a sudden drop of PRI immediately after a steep increase in light intensity. A slow phase of adjustment, after the initial rapid phase, lasts several minutes. The rapid phase is probably ascribable to chloroplast shrinkage following an increase of ΔpH and partly due to the non-photochemical quenching involving de-epoxidated xanthophylls; the slow phase is related to the latter phenomenon. Importantly, it has been proposed by Öquist and Huner (2003) that cold acclimation transforms the xanthophyll-mediated non-photochemical antenna quenching of absorbed light from a short-term dynamic response to a long-term sustained quenching for the whole winter period. This was supported by Ottander et al. (1995) who showed that the carotenoid content of Scots pine needles is subject to important accumulation during the cold season followed by a decrease when the full photosynthetic capacity is recovered in June. These changes were associated with a major reorganisation of the light-harvesting complexes. The pigment analysis conducted for this campaign confirmed a decrease of the carotenoid pool and especially of the lutein pigment during spring recovery. The good correlation found between the PRI and the net CO_2 assimilation would imply that PRI is also sensitive to this long-term sustained quenching. The steep increase of PRI in June correlates with the relaxation of that NPQ, and thus with the increase of the Scots pine photosynthetic activity.

The instrument required for the measurement of the PRI index is much simpler than that needed for measurement of CO_2 assimilation. PRI would then be an interesting alternative for the monitoring of photosynthetic activity at the tree canopy scale, over wide area.

The results presented here show that passive fluorescence remote sensing is now possible at the canopy level, at large distances and over a long period, even with cloudy weather. The 687/760 fluorescence ratio evolved parallel to the Chl content and a dynamical study of fluorescence showed the increase of photochemical activity. However, as the fluorescence signals strongly depend on structural effects, modeling will be necessary for further interpretation.

References

Adams, W. W., III, & Demmig-Adams, B. (1994). Carotenoid composition and down regulation of photosystem II in three conifer species during the winter. *Physiologia Plantarum*, *92*, 451–458.

Apostol, S., Briantais, J. -M., Moise, N., Cerovic, Z. G., & Moya, I. (2001). Photoinactivation of the photosynthetic electron transport chain by accumulation of over-saturating light pulses given to dark adapted pea leaves. *Photosynthesis Research*, *67*, 215–227.

Aurela, M., Laurila, T., & Tuovinen, J. -P. (2001). Seasonal CO2 balances of a subarctic mire. *Journal of Geophysical Research*, *106*(D2), 1623–1638.

Aurela, M., Laurila, T., & Tuovinen, J. -P. (2002). Annual CO_2 balance of a subarctic fen in northern Europe: The importance of the wintertime efflux. *Journal of Geophysical Research*, *107*(D21), 1–12.

Bilger, W., Björkman, O., & Thayer, S. S. (1989). Light-induced spectral absorbance changes in relation to photosynthesis and the epoxidation state of xanthophyll cycle components in cotton leaves. *Plant physiology*, *91*, 542–551.

Cerovic, Z. G., Goulas, Y., Gorbunov, M., Briantais, J. -M., Camenen, L., & Moya, I. (1996). Fluorosensing of water stress in plants. Diurnal changes of the mean lifetime and yield of chlorophyll fluorescence, measured simultaneously and at distance with a t-LIDAR and a modified PAM-fluorimeter, in maize, sugar beet and Kalanchoë. *Remote Sensing of Environment*, *58*, 311–321.

Demmig-Adams, B., & Adams, W. W. I. (1992). Photoprotection and other responses of plants to high light stress. *Annual Review of Plant Physiology and Plant Molecular Biology*, *43*, 599–626.

Evain, S., Camenen, L., & Moya, I. (2001). *Three channels detector for remote sensing of chlorophyll fluorescence and reflectance from vegetation, 8th international symposium: Physical measurements and signatures in remote sensing, Aussois, France, CNES, M. Leroy* (pp. 395–400).

Evain, S., Flexas, J., & Moya, I. (2004). A new instrument for passive remote sensing: 2. Measurement of leaf and canopy reflectance changes at 531 nm and their relationship with photosynthesis and chlorophyll fluorescence. *Remote Sensing of Environment*, *91*, 175–185.

Flexas, J., Briantais, J. -M., Cerovic, Z. G., Medrano, H., & Moya, I. (2000). Steady-state and maximum chlorophyll fluorescence responses to water stress in grapevine leaves: A new remote sensing system. *Remote Sensing of Environnment*, *73*, 283–297.

Gamon, J. A., Field, C. B., Bilger, W., Björkman, O., Fredeen, A. L., & Penuelas, J. (1990). Remote sensing of xanthophyll cycle and chlorophyll fluorescence in sunflower leaves and canopies. *Oecologia*, *85*, 1–7.

Gilmore, A. M., & Ball, M. C. (2000). Protection and storage of chlorophyll in overwintering evergreens. *Proceedings of the National Academy of Sciences*, *97*, 11098–11101.

Gitelson, A. A., Buschmann, C., & Lichtenthaler, H. K. (1999). The chlorophyll fluorescence ratio F735/F700 as an accurate measurement of the chlorophyll content in plants. *Remote Sensing of Environment*, *69*, 296–302.

Günther, K. P., Dahn, H. -G., & Lüdeker, W. (1994). Remote sensing vegetation status by laser-induced fluorescence. *Remote Sensing of Environment*, *47*, 10–17.

Hapke, B., DiMucci, D., Nelson, R., & Smythe, W. (1996). The cause of the hot spot in vegetation canopies and soils: Shadow-hiding versus coherent backscatter. *Remote Sensing of Environment*, *58*, 63–68.

Heber, U. (1969). Conformational changes of chloroplasts induced by illumination of leaves in vivo. *Biochimica et Biophysica Acta*, *180*, 302–319.

Heber, U., Neimanis, S., & Lange, O. L. (1986). Stomatal aperture, photosynthesis and water fluxes in mesophyll cells as affected by the abscission of leaves. Simultaneous measurements of gas exchange, light scattering and chlorophyll fluorescence. *Planta*, *167*, 554–562.

Ivanov, A. G., Sane, P., Zeilanov, Y., Malmberg, G., Gardeström, P., Huner, N. P. A., et al. (2001). Photosynthetic electron transport adjustments in overwintering Scots pine (*Pinus sylvestris* L.). *Planta*, *213*, 575–585.

Krause, G. H. (1973). The high-energy state of the thylakoid system as indicated by chlorophyll fluorescence and chloroplast shrinkage. *Biochimica et Biophysica Acta*, *292*, 715–728.

Kuusk, A. (1985). The hot spot effect of a uniform vegetative cover. *Soviet Journal of Remote Sensing*, *3*, 645–658.

Li, X. -P., Björkman, O., Shih, C., Grossman, A. R., Rosenquist, M., Jansson, S., et al. (2000). A pigment-binding protein essential for regulation of photosynthetic light harvesting. *Nature*, *403*, 391–395.

Moya, I., Camenen, L., Evain, S., Goulas, Y., Cerovic, Z. C., Latouche, G., et al. (2004). A new instrument for passive remote sensing: 1. Measurements of sunlight induced chlorophyll fluorescence. *Remote Sensing of Environment*, *91*, 186–197.

Moya, I., Camenen, L., Latouche, G., Mauxion, C., Evain, S., & Cerovic, Z. G. (1998). An instrument for the measurement of sunlight excited plant fluorescence. *Photosynthesis: Mechanisms and effects* (pp. 4265–4270). G. Garab, Dordrecht: Kluwer Academic Pub., V.

Niyogi, K. K. (1999). Photoprotection revisited: Genetic and molecular approaches. *Annual Review of Plant Physiology and Plant Molecular Biology*, *50*, 333–359.

Öquist, G., & Huner, N. P. A. (2003). Photosynthesis of overwintering evergreen plants. *Annual Review of Plant Biology*, *54*, 329–355.

Ottander, C., Douglas, C., & Öquist, G. (1995). Seasonal changes in photosystem II organisation and pigment composition in *Pinus sylvestris*. *Planta*, *197*, 176–183.

Plascyk, J. A. (1975). The MK II Fraunhofer line discriminator (FLD-II) for airborne and orbital remote sensing of solar-stimulated luminescence. *Optical Engineering*, *14*, 339–346.

Plascyk, J. A., & Gabriel, F. C. (1975). The Fraunhofer line discriminator MKII-An airborne instrument for precise and standardized ecological luminescence measurements. *IEEE Transactions on Instrumentation and Measurement*, *24*, 306–313.

Ruban, A. V., Horton, P., & Young, A. J. (1993). Aggregation of higher plant xanthophylls—differences in absorption spectra and in the dependency on solvent polarity. *Journal of Photochemistry and Photobiology, B, Biology*, *21*, 229–234.

Tucker, C. J. (1979). Red and photographic infrared linear combination for monitoring vegetation. *Remote Sensing of Environment*, *8*, 127–150.